PRAMANA — journal of physics

Vol. 83, No. 4
October 2014
pp. 557–570

Immiscible multicomponent lattice Boltzmann model for fluids with high relaxation time ratio

TAO JIANG, QIWEI GONG*, RUOFAN QIU and ANLIN WANG
College of Mechanical Engineering, Tongji University, 4800# Cao'an Road, Shanghai 201804, China
*Corresponding author. E-mail: 2012gongqiwei@tongji.edu.cn

MS received 9 October 2013; revised 6 February 2014; accepted 7 February 2014
DOI: 10.1007/s12043-014-0805-7; ***e*Publication:** 5 August 2014

Abstract. An immiscible multicomponent lattice Boltzmann model is developed for fluids with high relaxation time ratios, which is based on the model proposed by Shan and Chen (SC). In the SC model, an interaction potential between particles is incorporated into the discrete lattice Boltzmann equation through the equilibrium velocity. Compared to the SC model, external forces in our model are discretized directly into the discrete lattice Boltzmann equation, as proposed by Guo *et al.* We develop it into a new multicomponent lattice Boltzmann (LB) model which has the ability to simulate immiscible multicomponent fluids with relaxation time ratio as large as 29.0 and to reduce 'spurious velocity'. In this work, the improved model is validated and studied using the central bubble case and the rising bubble case. It finds good applications in both static and dynamic cases for multicomponent simulations with different relaxation time ratios.

Keywords. Multicomponent; high relaxation time ratio; lattice Boltzmann method.

PACS Nos 47.11.–j; 47.54.Bd; 02.70.–c

1. Introduction

Multicomponent systems are part of many natural physical processes, especially gas–liquid systems and they are widely used in industry for various purposes. For example, gas is released into liquid phase to form small bubbles in boling-water reactors for cooling the fusion core, in bubble column reactors for chemical reactions, and in boilers for producing steam [1].

During the past decade, the lattice Boltzmann equation (LBE) method [2,3] has emerged as a new promising method of computational fluid dynamics (CFD). This method was developed from a discretized fluid model known as the lattice gas automata (LGA) [4,5]. Since Rothman and Keller introduced the first LGA model for simulation of two immiscible fluids, several lattice Boltzmann (LB) models have been constructed

for simulating immiscible fluids, such as the interaction potential approach [6], the free engery approach [7] and so on.

The model proposed by Shan and Chen (SC) is one of the most popular models for multicomponent simulations [8,9]. In the SC model, an interaction potential between particles is incorporated into the discrete lattice Boltzmann equation through the equilibrium velocity. Thus, the SC forces can cause components separation, when the interaction strength is properly adjusted [6,10]. However, when it comes to simulations for multicomponent immiscible fluids with relaxation time ratios larger than 1.0, the SC model is not useful because the magnitude of the 'spurious velocity' is too large at the interface, which causes the SC model to be unstable during the evolution. But in physical and chemical applications, mixed fluids are very common and they are usually of different values of relaxation time and the relaxation time ratios of the components could vary in a wide range.

In this work, we present an improved LB model for immiscible multicomponent fluids with relaxation time ratios much larger than 1.0. In §2, we briefly review the LBE method, the SC forcing term and then we introduce the improved LB model in detail. In §3, we first conduct a static numerical simulation to verify the improved LB model according to the Laplace's law and next, we compare the static features of SC model and the improved LB model including the maximum relaxation time ratio and the 'spurious velocity' through the central bubble case. Then, we perform a series of simulations to validate the dynamic applicability of the improved LB model through the single bubble rising case. In §4, we reach a conclusion about the improved LB model and describe its future application, according to the simulation results.

2. LBE method

The discrete lattice Boltzmann equation using the BGK collision term without the forcing term for multicomponent flows can be described as follows [11]:

$$f_\alpha^\sigma(\mathbf{x}+\mathbf{e}_\alpha\delta_t, t+\delta_t) - f_\alpha^\sigma(\mathbf{x}, \mathrm{t}) = -\frac{1}{\tau^\sigma}\left[f_\alpha^\sigma(\mathbf{x}, t) - f_\alpha^{\mathrm{eq},\sigma}(\mathbf{x}, t)\right], \tag{1}$$

where f_α^σ is the distribution function of the σth component for particles along the αth direction and $f_\alpha^{\mathrm{eq},\sigma}$ is its corresponding equilibrium distribution function, $\mathbf{e}_\alpha$ is the particle velocity in the αth direction, δt is the time step and τ^σ is the single relaxation time of the σth component.

In this work, we would like to use the D2Q9 model which has nine directions of velocities on the two-dimensional square lattice.

The discrete velocities of the D2Q9 model are given as follows [12]:

$$\mathbf{e}_\alpha = \begin{cases} (0,0), & \alpha = 0, \\ c\left(\cos\left[(\alpha-1)\pi/2\right], \sin\left[(\alpha-1)\pi/2\right]\right), & \alpha = 1,2,3,4, \\ \sqrt{2c}\left(\cos\left[(2\alpha-1)\pi/4\right], \sin\left[(2\alpha-1)\pi/4\right]\right), & \alpha = 5,6,7,8. \end{cases} \tag{2}$$

Based on the frame definitions of the D2Q9 model, the equilibrium function for the multicomponent flows can be introduced as follows:

$$f_\alpha^{\mathrm{eq},\sigma} = \omega_\alpha \rho^\sigma \left[1 + \frac{\mathbf{e}_\alpha \cdot \mathbf{u}^{\mathrm{eq},\sigma}}{c_\mathrm{s}^2} + \frac{(\mathbf{e}_\alpha \cdot \mathbf{u}^{\mathrm{eq},\sigma})^2}{2c_\mathrm{s}^4} - \frac{(\mathbf{u}^{\mathrm{eq},\sigma})^2}{2c_\mathrm{s}^2} \right], \tag{3}$$

where ω_α is the weighing factor, $\rho^\sigma = \sum_\alpha f_\alpha^\sigma$ is the local mass density, $c_\mathrm{s} = 1/\sqrt{3}$ is the lattice sound speed and $\mathbf{u}^{\mathrm{eq},\alpha}$ is the equilibrium velocity of the σth component.

The weighing factor ω_α is given as follows:

$$\omega_\alpha = \begin{cases} 4/9, & \alpha = 0, \\ 1/9, & \alpha = 1, 2, 3, 4, \\ 1/36, & \alpha = 5, 6, 7, 8. \end{cases} \tag{4}$$

In the absence of interparticle forces, all components are ideal gases [13]. Thus, all of the equilibrium velocities $\mathbf{u}^{\mathrm{eq},\sigma}$ are equal to a common velocity, $\mathbf{u}'$. To conserve the total momentum of particles of all components, the common velocity is given as

$$\mathbf{u}' = \frac{\sum_\sigma \rho^\sigma \mathbf{u}^\sigma / \tau^\sigma}{\sum_\sigma \rho^\sigma / \tau^\sigma}, \tag{5}$$

where $\rho^\sigma \mathbf{u}^\sigma = \sum_\alpha f_\alpha^\sigma \mathbf{e}_\alpha$ is the momentum of the σth component.

2.1 *SC forcing term*

To segregate an immiscible fluid system into different components, Shan and Chen [6] introduced a long-range force between particles of component σ at site $\mathbf{x}$ and particles of component $\bar{\sigma}$ at site $\mathbf{x}'$. It is given below [13]:

$$\mathbf{F}^\sigma(\mathbf{x}) = -\psi^\sigma(\mathbf{x}) \sum_{\mathbf{x}'} \sum_{\bar{\sigma}} G_{\sigma\bar{\sigma}} \left(\mathbf{x}, \mathbf{x}'\right) \psi^{\bar{\sigma}} \left(\mathbf{x}'\right) \left(\mathbf{x}' - \mathbf{x}\right), \tag{6}$$

where $\psi^\sigma(\mathbf{x})$ is the 'effective mass' of the σth component at site $\mathbf{x}$ and it is defined as a function of the local mass density ρ^σ and $G_{\sigma\bar{\sigma}}\left(\mathbf{x}, \mathbf{x}'\right)$ is the Green's function.

Due to the interparticle force, an extra momentum change to the σth component is added to the momentum change caused by collision with others. Thus, the momentum is adjusted for each component as [13]

$$\rho^\sigma \mathbf{u}^{\mathrm{eq},\sigma} = \rho^\sigma \mathbf{u}' + \tau^\sigma \mathbf{F}^\sigma. \tag{7}$$

Using eqs (5) and (7), the total momentum of the fluid mixture is given below:

$$\rho \mathbf{u} = \sum_\sigma \rho^\sigma \mathbf{u}^\sigma + \frac{1}{2} \sum_\sigma \mathbf{F}^\sigma, \tag{8}$$

where $\rho = \sum_\sigma \rho^\sigma$ is the total mass density of the fluid.

2.2 *The improved LB model*

Compared to the SC model, the discrete forcing term of the improved LB model is directly incorporated into the discrete lattice Boltzmann equation [14]. Thus, the equation is developed for multicomponent flow as follows:

$$f_\alpha^\sigma(\mathbf{x}+\mathbf{e}_\alpha\delta_t, t+\delta_t) - f_\alpha^\sigma(\mathbf{x}, t) = \delta_t F_\alpha^\sigma - \frac{1}{\tau^\sigma}\left[f_\alpha^\sigma(\mathbf{x}, t) - f_\alpha^{\mathrm{eq},\sigma}(\mathbf{x}, t)\right], \quad (9)$$

where F_α^σ is the discrete forcing term of the σth component and it is defined for multicomponent fluid as follows [14]:

$$F_\alpha^\sigma = \left(1 - \frac{1}{2\tau^\sigma}\right)\omega_\alpha\left[\frac{\mathbf{e}_\alpha - \mathbf{u}^{\mathrm{eq}}}{c_\mathrm{s}^2} + \frac{(\mathbf{e}_\alpha\cdot\mathbf{u}^{\mathrm{eq}})}{c_\mathrm{s}^4}\mathbf{e}_\alpha\right]\cdot\mathbf{F}^\sigma, \quad (10)$$

where $\mathbf{F}^\sigma$ is the external force and $\mathbf{u}^{\mathrm{eq}}$ is the equilibrium velocity of the fluid mixture.

According to the discete LBE with discrete forcing term above, the local mass density of the σth component and its corresponding momentum are given as follows:

$$\rho^\sigma = \sum_\alpha f_\alpha^\sigma, \quad (11)$$

$$\rho^\sigma\mathbf{u}^\sigma = \sum_\alpha f_\alpha^\sigma\mathbf{e}_\alpha + \frac{\delta_t}{2}\mathbf{F}^\sigma. \quad (12)$$

We can see that the momentum of the σth component in eq. (12) consists of the momentum change caused by the external forces, due to the discrete forcing term in eq. (9). In the SC model, the momentum of the σth component is defined in eq. (5), in the absence of interparticle forces.

To calculate the discrete forcing term in eq. (10) and the equilibrium distribution function for multicomponent flows, we need to aquire the equilibrium velocity of the fluid mixture. It is given as follows:

$$\mathbf{u}^{\mathrm{eq}} = \frac{\sum_\sigma \rho^\sigma\mathbf{u}^\sigma/\tau^\sigma}{\sum_\sigma \rho^\sigma/\tau^\sigma}. \quad (13)$$

The improved LB model directly add the forcing term to the discrete lattice Boltzmann equation, rather than the SC model which introduces the external force effects to the equation through the equilibrium velocity of each component, $\mathbf{u}^{eq,\sigma}$. Thus, you would notice that in eq. (10), we use the equilibrium velocity, $\mathbf{u}^{eq}$ to calculate the discrete forcing term, rather than the equilibrium velocity of each component, $\mathbf{u}^{eq,\sigma}$.

The equilibrium function of the σth component is given below, and the velocity is also replaced by the equilibrium velocity of the fluid mixture, $\mathbf{u}^{eq}$:

$$f_\alpha^{eq,\sigma} = \omega_\alpha\rho^\sigma\left[1 + \frac{\mathbf{e}_\alpha\cdot\mathbf{u}^{eq}}{c_s^2} + \frac{(\mathbf{e}_\alpha\cdot\mathbf{u}^{eq})^2}{2c_s^4} - \frac{(\mathbf{u}^{eq})^2}{2c_s^2}\right]. \quad (14)$$

Using eqs. (11) and (12), the total momentum of the fluid mixture is given as follows:

$$\rho\mathbf{u} = \sum_\sigma \rho^\sigma\mathbf{u}^\sigma, \quad (15)$$

where $\rho = \sum_\sigma \rho^\sigma$ is the total mass density of the fluid.

3. Numerical simulation results

In SC's original paper, the external force in eq. (6) is derived by using the interparticle forces of the nearest-neighbour sites. In this work, we adopt the external force which is extended to include other neighbour sites [15]. Therefore, it is given in the following form:

$$\mathbf{F}^{\sigma}(\mathbf{x}) = -c_0\psi^{\sigma}(\mathbf{x})\sum_{\bar{\sigma}} g_{\sigma\bar{\sigma}}\nabla\psi^{\bar{\sigma}}(\mathbf{x}), \tag{16}$$

where c_0 is a constant and $c_0 = 6.0$ is given for the D2Q9 model.

Under the definition of $\mathbf{F}^{\sigma}$ in eq. (16), p is the pressure given as function of all the densities of all the components by the following equation of state of the system [13,15]:

$$p = \rho c_s^2 + \frac{c_0}{2}\sum_{\sigma\bar{\sigma}} g_{\sigma\bar{\sigma}}\psi^{\sigma}\nabla\psi^{\bar{\sigma}}, \tag{17}$$

where $\rho = \sum_{\sigma}\rho^{\sigma}$ is the total mass density of the fluid.

To calculate the gradient term in eq. (16), we could use the nearest sites or both the nearest and next-nearest sites, which is shown in figure 1.

As we know, the stability can be improved at a higher isometry via more neighbouring points. So, we plot the velocity distributions of the two methods in figure 2 to compare the 'spurious velocity' using the central bubble model.

'Spurious velocity' [16–18] is known as a small but finite-amplitude circulating flow near the interface of a stationary bubble. It causes instability of the LB models in the evolution of the numerical simulations.

In this case, we assume that the conditions of the two methods are the same.

Figure 2 shows the velocity distribution at each lattice site of the two methods. We can see that the largest velocity occurs at the interface of the central bubble, which is known as the 'spurious velocity'. It is obvious that the 'spurious velocity' of the method using the nearest sites is much larger than the other one.

Therefore, we use both the nearest and next-nearest sites to calculate the gradient term in eq. (16), which gives a six-point scheme for two dimension. It is introduced as follows [15]:

$$\begin{aligned}\frac{\partial\psi(i,j)}{\partial x} &= c_1\big[\psi(i+1,j)-\psi(i-1,j)\big]\\ &\quad + c_2\big[\psi(i+1,j+1)-\psi(i-1,j+1)\\ &\quad + \psi(i-1,j+1)-\psi(i-1,j-1)\big],\end{aligned} \tag{18}$$

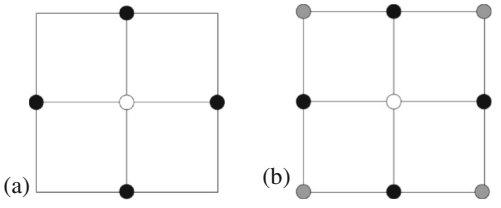

Figure 1. The sites used in the calculation of the gradient term. (**a**) Nearest sites and (**b**) nearest and next-nearest sites.

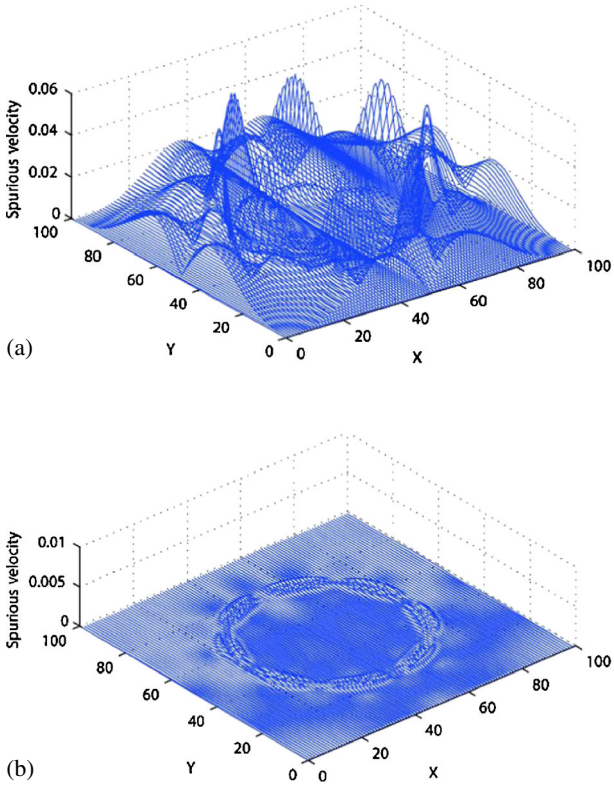

Figure 2. Velocity distribution at each lattice site of the two methods. (**a**) Nearest sites and (**b**) nearest and next-nearest sites.

$$\frac{\partial \psi(i,j)}{\partial y} = c_1\big[\psi(i,j+1) - \psi(i,j+1)\big] + c_2\big[\psi(i+1,j+1) - \psi(i+1,j-1) + \psi(i-1,j+1) - \psi(i-1,j-1)\big], \tag{19}$$

where c_1 and c_2 are weighing coefficients for the nearest and next-nearest sites, respectively, and $c_1 = 4c_2 = 1/3$ is given for the D2Q9 model.

To validate the improved LB model introduced above, we perform several numerical simulations using the central bubble case and the single bubble rising case, respectively.

3.1 *Static cases*

The case of central bubble which we use, contains two kinds of immiscible fluid components. One is a circular bubble located at the centre of a domain containing the other component initially. We suggest that the subscripts 1 and 2 refer to the bubble in the centre and the domain around the bubble, respectively. And we apply periodic boundary to all the numerical simulations in the case of central bubble.

3.1.1 *Laplace's law.* According to the Laplace's law, the pressure difference and the surface tension are given for the two-dimensional circular bubble as follows:

$$p_1 - p_2 = \frac{\sigma}{R}, \tag{20}$$

where p_1 and p_2 are the pressures of the first and second component defined above, respectively, σ is the surface tension and R is the radius of the circular bubble in the centre.

In this case, the radius of the central bubble ranges from 25 to 40 lattice sites and the domain around contains 100×100 lattice sites. We perform three groups of numerical simulations when the values of relaxation time ratio τ_1/τ_2 are 1, 5 and 25, respectively.

Figure 3 shows the relation between the pressure difference $p_1 - p_2$ and the reciprocal of radius R at different relaxation time ratios, τ_1/τ_2. The dots represent the statistics we obtain from the numerical simulations and the lines are the least-square fit lines we use to approximate the statistics. Thus, the slope means the surface tension of each group.

We can see that the lines match the statistics well and the results agree with the Laplace's law within the accuracy of our measurement. It suggests that the improved LB model we introduce is an available LB model for immiscible multicomponent fluids simulation.

3.1.2 *Comparison between SC and the improved LB model.* To show the advantages of the improved LB model over SC model in multicomponent flow simulations, we conduct two kinds of numerical simulations between the two models. In the following simulations, we set the radius of the circular bubble as $R = 40$ lattice sites and the domain contains 100×100 lattice sites as well.

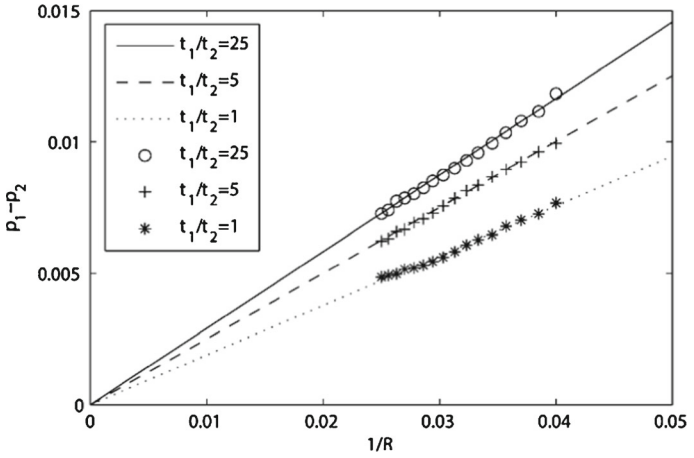

Figure 3. Verification of Laplace's law for the improved LB model at different relaxation time ratios, τ_1/τ_2.

First, we perform a simulation to compare the maximum relaxation time ratio that the two models can simulate at the same condition. We assume that the relaxation time of the second component τ_2 in the two models is the same in this simulation.

Figure 4 shows the comparison of the maximum relaxation time ratio $(\tau_1/\tau_2)_{\max}$ that the two models can simulate, when they are of the same relaxation time τ_2.

Because of the limitation of the SC model, we can see from figure 4 that the relaxation time τ_2 has a narrow range from just 0.93 to 1.60. The maximum relaxation time ratio $(\tau_1/\tau_2)_{\max}$ is only about 3.0 for the SC model, whereas the improved LB model is capable of simulations for much larger relaxation time ratio at the same τ_2. We can see from figure 4 that the maximum relaxation time ratio $(\tau_1/\tau_2)_{\max}$ of the improved LB model is above 20.0 for τ_2 from 0.93 to 1.60.

Next, we conduct another group of simulations to compare the 'spurious velocity' of the two models.

Figure 5 shows the velocity distribution at each lattice site of the two models. In this case, the relaxation time ratio τ_1/τ_2 is set as 1.0. We can see that the 'spurious velocity' of the SC model is much larger than that of the improved LB model.

Figure 6 shows the comparison of the magnitude of the 'spurious velocity' between the two models at different relaxation time, τ_2.

Due to the limitations of the SC model, we still restrict the relaxation time τ_2 from 0.93 to 1.60. We can see from figure 6 that the magnitude of 'spurious velocity' in the improved LB model is approximately 10^{-3} and in the SC model it is around 10^{-1}. Therefore, the improved LB model is obviously more stable than the SC model, because of the drastically reduced value of 'spurious velocity'.

Above all, we find that the improved LB model is an available multicomponent LB model, according to the Laplace's law. It is much more stable in numerical simulations than the SC model, because of the decrease in the 'spurious velocity'. Therefore, the improved LB model we suggest is capable and stable for immiscible multicomponent fluid simulations under static cases.

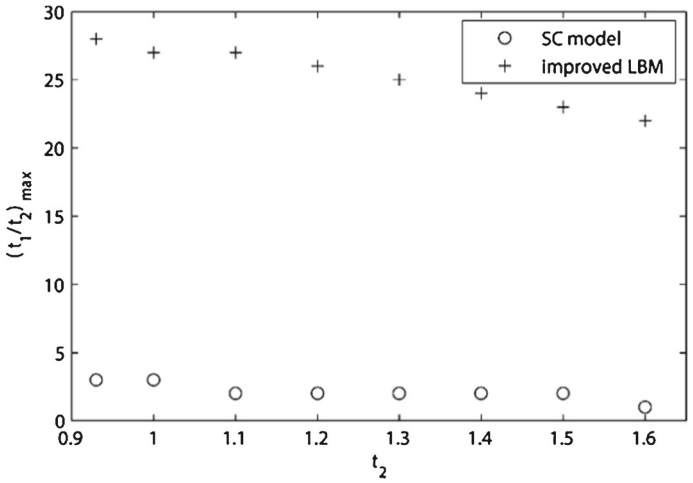

Figure 4. Comparison between the SC and the improved LB model for the maximum relaxation time ratio $(\tau_1/\tau_2)_{\max}$ at the same value of the relaxation time τ_2.

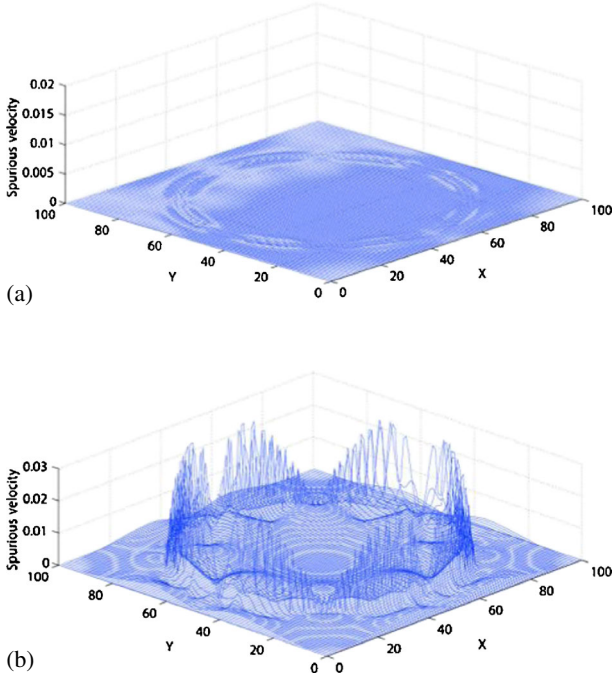

Figure 5. Velocity distribution at each lattice site of (**a**) the improved LB model and (**b**) the SC model.

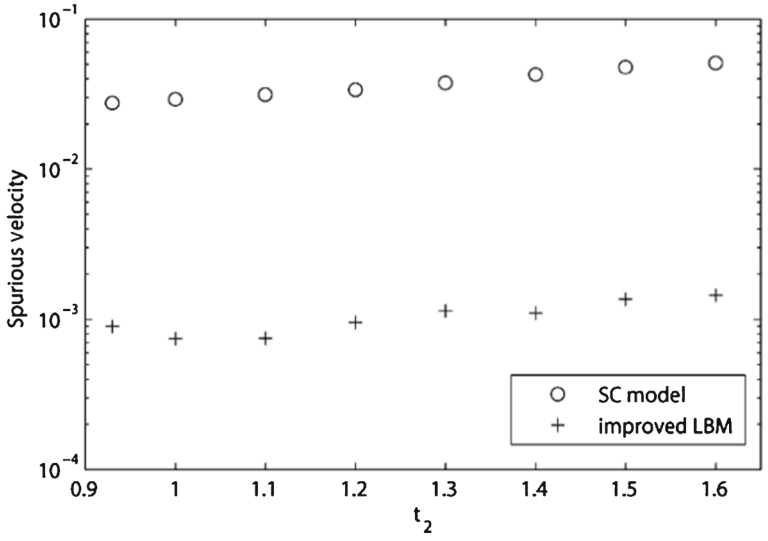

Figure 6. Comparison of 'spurious velocity' between the two models at different relaxation time τ_2.

3.1.3 *Properties of the improved LB model.* In the following, we conduct a group of simulations to further study the static applicability of the improved LB model using the central bubble case. We still set the radius of the circular bubble as $R = 40$ lattice sites and the domain also contains 100×100 lattice sites.

Figure 7 shows the maximum relaxation time ratio $(\tau_1/\tau_2)_{\max}$ that the improved LB model can simulate at a wide range of the relaxation time, τ_2.

Due to the stability of the improved LB model, we find that the improved LB model is capable of simulations for a much larger range of relaxation time τ_2 than that of the SC model.

We can see from figure 7 that the relaxation time τ_2 ranges from 0.501 to 14.0 in this case. For different relaxation time τ_2, the maximum relaxation time ratio $(\tau_1/\tau_2)_{\max}$ varies from 1.0 to 29.0. While the value of the relaxation time τ_2 in this case is less than 1.0, the maximum relaxation time ratio $(\tau_1/\tau_2)_{\max}$ increases rapidly as the relaxation time τ_2 become larger. While the relaxation time τ_2 reaches a value of 1.0, the maximum relaxation time ratio $(\tau_1/\tau_2)_{\max}$ reaches a value of 29.0. However, the maximum relaxation time ratio $(\tau_1/\tau_2)_{\max}$ decreases rapidly as the value of the relaxation time τ_2 deviates away from 1.0.

Therefore, we can conclude that the improved LB model we proposed is an available and stable LB model for multicomponent flows with a high relaxation time ratio.

3.2 *Dynamic cases*

We perform several simulations to study the bubble motion. The rising bubble case, we use contains two kinds of immiscible fluid components. One is a circular bubble located at the bottom of a domain containing the other component initially. We suggest that the subscripts 1 and 2 refer to the bubble and the domain around the bubble, respectively.

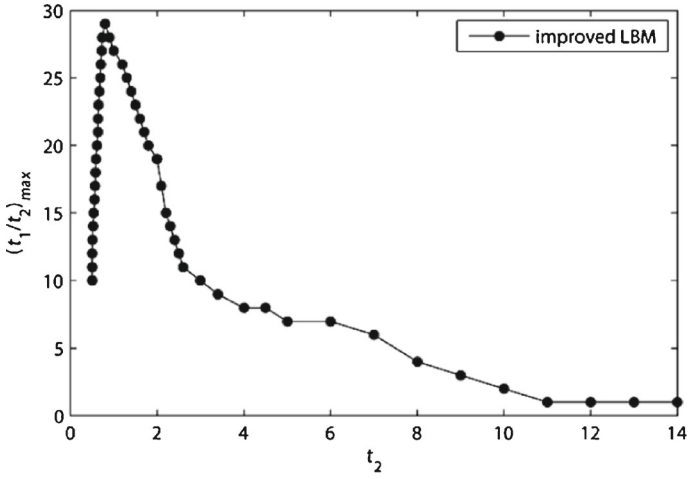

Figure 7. The maximum relaxation time ratio $(\tau_1/\tau_2)_{\max}$, the improved LB model can reach, at different relaxation time τ_2.

The most important dimensionless parameters in the study of bubble motion are Eotvos number (Eo), Motorn number (Mo) and Reynolds number (Re) [19].

Eo represents the dimensionless size of the bubble and it determines the amount of the deformation of a rising bubble. It is defined as

$$\mathrm{Eo} = \frac{g\Delta\rho d_\mathrm{e}^2}{\sigma}, \tag{21}$$

where g is the acceleration due to gravity, $\Delta\rho$ is the difference in density between the domain and bubble, d_e is the effective diameter of the bubble and σ is the surface tension.

Mo characterizes the properties of the fluid system surrounding the bubble. It is defined as

$$\mathrm{Mo} = \frac{g\rho_2^2\Delta\rho\upsilon_2^4}{\sigma^3}, \tag{22}$$

where ρ_2 is the density of the domain around the bubble and υ_2 is the viscosity of the domain.

The flow field around the bubble is determined by the Reynolds number, which is defined as

$$\mathrm{Re} = \frac{U_\mathrm{t} d_\mathrm{e}}{\upsilon_2} \tag{23}$$

where U_t is the terminal velocity of the rising bubble. It determines the Reynolds number of the flow.

In the following, we set the initial diameter of the bubble as 14 lattice sites and the domain around the bubble contains 150 $\times$ 300 lattice sites. The bubble initially located at the site (75,40). To keep the bubble motion away from the walls, periodic boundary condition is imposed at all the boundaries of the domain.

In this case, we determine the surface tension of the bubble in a stationary fluid without gravity according to the Laplace's law. And the terminal velocity is calculated through the lattice sites which the bubble rises across and the time steps in the evolution.

When the bubble is in equilibrium for a long time in the domain, a steady state is achieved, and then gravity is switched on. The gravitational force is in the negative vertical direction. Sankaranarayanan *et al* [20] have suggested that this external force can be introduced into the force equation using the expression given below:

$$\mathbf{a}_\mathrm{ext} = \mathbf{g}\left(1 - \frac{\langle\rho\rangle}{\rho}\right), \tag{24}$$

where ρ is the number density of the mixture at the node of interest and $\langle\rho\rangle$ is the average number density of the mixture in the entire domain.

For the first case, we set the relaxation time the same for the two components. For a series of values of Eo and Mo, we perform a variety of simulations to validate the dynamic property of the improved LB model. When the rising bubble reached a steady state, we can calculate the terminal velocity of the rising bubble. Hence, we can determine the Reynolds number of the flow of bubble motion.

To validate the improved LB model, we compare the shape of the bubble and the Reynolds number with the bubble regime map constructed by Grace [21] according to the values of Eo and Mo, and we plot several typical cases in figure 8.

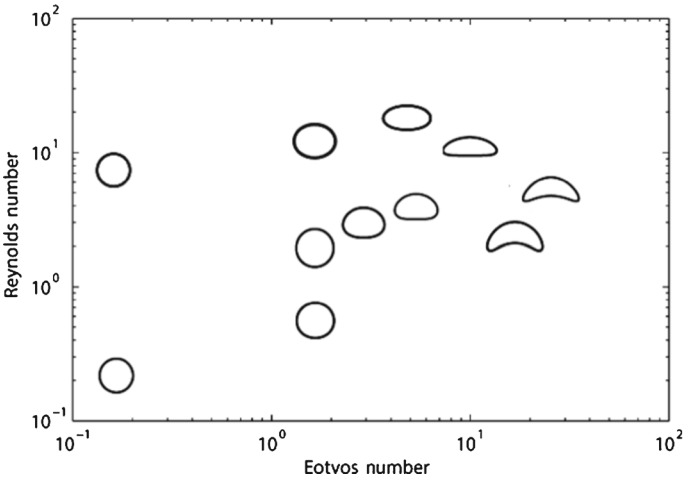

Figure 8. Bubble shape map at the same relaxation time of the two components.

We can see from figure 8 that the shape of the bubble and Reynolds number are consistent with the bubble map proposed by Grace [21]. Therefore, we can conclude that the improved LB model we propose is an available multicomponent LB model for simulating dynamic cases.

The details of the parameters of the first case are showed in table 1.

In the second case, we perform several simulations to see the applicability of the improved LB model for different relaxation time ratios for dynamic cases. We set the relaxation time of the bubble as 6.0 and that of the domain around the bubble as 0.6, 1.2 and 2.0. That means, we set the relaxation time ratios as 10, 5 and 3 to study the dynamic property of the improved LB model at different relaxation time ratios. We also compare

Table 1. Parameters for a rising bubble at the same relaxation time of the two components.

τ_1	τ_2	Eo	Mo	Re	Shape
0.6	0.6	0.16	7.94×10^{-8}	7.45	Spherical
0.75	0.75	1.64	3.42×10^{-5}	12.31	Oblate ellipsoid
0.75	0.75	4.91	1.03×10^{-4}	18.36	Oblate ellipsoid
1.0	1.0	9.98	3.45×10^{-3}	10.80	Oblate ellipsoid
1.5	1.5	0.17	9.33×10^{-4}	0.22	Spherical
1.5	1.5	1.67	9.33×10^{-3}	2.00	Spherical
1.5	1.5	3.01	1.68×10^{-2}	2.97	Oblate ellipsoid
1.5	1.5	5.02	2.80×10^{-2}	3.78	Oblate ellipsoid
2.0	2.0	25.10	7.08×10^{-1}	5.4	Oblate ellipsoid cap
2.5	2.5	1.67	1.48×10^{-1}	0.57	Spherical
2.5	2.5	6.71	1.48	2.43	Oblate ellipsoid cap

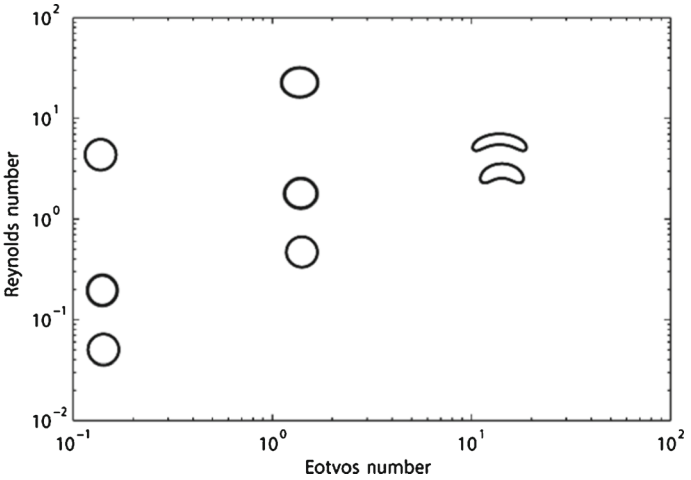

Figure 9. Bubble shape regime map at different relaxation time ratios.

the bubble shape and the Reynolds number with the bubble regime map of Grace [21] at the same values of Eo and Mo and plot the typical results in figure 9.

The details of the parameters of the second case are showed in table 2.

We can see from figure 9 that the bubble shape and Reynolds number are also consistent with the bubble map proposed by Grace [21]. Therefore, we believe that the improved LB model is still capable of simulation for bubble motion at different relaxation time ratios.

Above all, the figures and tables show that the current numerical simulation using the improved LB model performs excellent quantitative and qualitative results for a single rising bubble simulation. Bubble shapes and the Reynolds number in both cases are consistent with Grace's bubble shape map. Therefore, we can conclude that the improved LB model that we proposed is also an available LB model for multicomponent flows with a high relaxation time ratio under dynamic cases.

Table 2. Parameters for a rising bubble at different relaxation time ratios of the two components.

τ_1	τ_2	Eo	Mo	Re	Shape
6.0	0.6	0.14	2.22×10^{-7}	4.31	Spherical
6.0	0.6	1.37	2.22×10^{-6}	23.20	Oblate ellipsoid
6.0	1.2	0.14	5.53×10^{-4}	0.20	Spherical
6.0	1.2	1.39	5.53×10^{-3}	1.80	Oblate ellipsoid
6.0	1.2	13.91	5.53×10^{-2}	6.21	Oblate ellipsoid cap
6.0	2.0	0.14	1.20×10^{-2}	0.05	Spherical
6.0	2.0	1.41	1.20×10^{-1}	0.48	Spherical
6.0	2.0	14.10	1.20	2.9	Oblate ellipsoid cap

4. Conclusion

This work shows that the improved LB model is much more stable than SC model in multicomponent flow simulations due to the way we introduce the external forces into the discrete lattice Boltzmann equation and we define velocity in the discrete forcing term. The improved LB model is capable of simulating for a much wider relaxation time values ranging from 0.501 to 14.0 and improving the maximum relaxation time ratio to a value as large as 29.0. Besides, for the dymanic cases of multicompenent systems, the improved LB model finds many application at different relaxation time ratios.

Above all, we can see that the improved LB model is probably used for simulations of different kinds of immiscible fluid mixtures at different temperatures and pressures.

Acknowledgement

This work is supported by National Natural Science Foundation of China under Grant No. 51178347.

References

[1] I O Kurtoglu and C Lin, *Numer. Heat. Tr. B-fund.* **50**, 333 (2006)
[2] A Dupuis and J M Yeomans, *Pramana – J. Phys.* **64**,1019 (2005)
[3] S Ryu and S Ko, *Nucl. Eng. Des*. **248**, 248 (2012)
[4] U Frisch, B Hasslacher and Y Pomeau, *Phys. Rev. Lett.* **56**, 1505 (1986)
[5] S Wolfram, *J. Stat. Phys.* **45**, 471 (1986)
[6] X Shan and H Chen, *Phys. Rev. E* **47**, 1815 (1993)
[7] M R Swift, E Orlandini, W R Osborn and J M Yeomans, *Phys. Rev. E* **54**, 5041 (1996)
[8] M Sbragaglia, R Benzi, L Biferale, S Succi, K Sugiyama and F Toschi, *Phys. Rev. E* **75**, 26702 (2007)
[9] S Chibbaro, G Falcucci, G Chiatti, H Chen, X Shan and S Succi, *Phys. Rev. E* **77**, 036705 (2008)
[10] X Shan and H Chen, *Phys. Rev. E* **49**, 2941 (1994)
[11] P L Bhatnagar, E P Gross and M Krook, *Phys. Rev*. **94**, 511 (1954)
[12] Y H Qian, D D'Humieres and P Lallemand, *Europhys. Lett.* **17**, 479 (1992)
[13] X Shan and G Doolen, *J. Stat. Phys.* **81**, 379 (1995)
[14] Z Guo, C Zheng and B Shi, *Phys. Rev. E* **65**, 046308 (2002)
[15] P Yuan and L Schaefer, *Phys. Fluids* **18**, 42101 (2006)
[16] A J Wagner, *Int. J. Mod. Phys. B* **17**, 193 (2003)
[17] X Shan, *Phys. Rev. E* **73**, 047701 (2006)
[18] C M Pooley and K Furtado, *Phys. Rev. E* **77**, 046702 (2008)
[19] A Gupta and R Kumar, *Int. J. Heat Mass Transfer* **51**, 5192 (2008)
[20] K Sankaranarayanan, X Shan, I G Kevrekidis and S Sundaresan, *J. Fluid Mech.* **452**, 61 (2002)
[21] J R Grace, *Trans. Inst. Chem. Eng.* **51**, 116 (1973)